JOURNAL OF SPACECRAFT AND ROCKETS
Vol. 29, No. 2, March-April 1992

Effects of Shock Wave Precursors Ahead of Hypersonic Entry Vehicles

Scott A. Stanley*
Lockheed Engineering and Sciences Company, Houston, Texas 77058
and
Leland A. Carlson†
Texas A&M University, College Station, Texas 77843

A model has been developed to predict the magnitude and characteristics of the shock wave precursor ahead of a hypervelocity vehicle entering the Earth's atmosphere. This model includes both chemical and thermal nonequilibrium, utilizes detailed mass production rates for the photodissociation and photoionization reactions, and accounts for the effects of radiative absorption and emission on the individual internal energy modes of both atomic and diatomic species. For this study, the Earth's atmosphere is modeled as pure nitrogen rather than as a nitrogen oxygen mixture. Comparison of the present results with shock tube data indicates that the model is reasonably accurate. A series of test cases representing Earth aerocapture return from Mars indicate that there is a significant production of atoms, ions, and electrons ahead of the shock front due to radiative absorption and that the precursor is characterized by an enhanced electron/electronic temperature and molecular ionization. However, the precursor has a negligible effect on the shock layer flowfield.

Nomenclature

AF = radiation attenuation factor
D_n = dissociation energy for the nth species, eV
E = energy per particle, eV
E_3 = third exponential integral
e = energy per unit mass, erg/g
e_e'' = electron/electronic energy, erg/g
H = total enthalpy, erg/g
h = static enthalpy, erg/g
$h\nu$ = photon energy, eV
I_i = ionization energy of the ith species, eV
k = Boltzmann's constant, 1.38×10^{-16} erg/K
k'_ν = absorption coefficient, 1/cm
M_n = molecular weight of the nth species, g/mole
m_n = mass per particle of the nth species, g
N_n = number density of the nth species, 1/cm^3
n_{diss} = number of bound-free dissociation processes
n_{mb} = number of molecular bands
n_s = number of species
p = pressure, dyne/cm^2
q = radiative flux, W/cm^2
$\bar{R}$ = universal gas constant, 8.317×10^7 erg/K g mole
T = heavy particle temperature, K
T_e = electron/electronic temperature, K
V = velocity, cm/s
$\dot{w}_n$ = mass production rate of the nth species, g/cm^3 s
x = spatial variable in the precursor, cm
Y = absorption coefficient ratio
β = one-half of the angle subtended by the body
ν = frequency, 1/s
ξ = energy production due to inelastic collisions, W/cm^3
ρ = density, g/cm^3
τ = optical depth

Subscripts
elct = electronic
i = for the ith process
j = for the jth electronic level
n = for the nth species
rot = rotational
tr = translational
vib = vibrational
ν = at the frequency ν

Superscripts
TS = tangent slab approximation
s = at the shock

Introduction

THE recent emphasis placed on a mission to Mars and the subsequent return of samples has caused an increased interest in the development of accurate methods for predicting the fluid flow around hypersonic entry vehicles. This interest is a result of the plan to use an aerocapture technique to provide the reduction in velocity necessary to place the spacecraft in Earth orbit. This technique uses aerodynamic drag, resulting from the interaction of the spacecraft with the Earth's atmosphere, instead of propulsive braking to slow the vehicle to orbital speeds. Such an approach provides a reduction in the fuel necessary for the mission and an increase in the payload capabilities. A vehicle entering the Earth's atmosphere upon return from Mars will experience velocities in the high hypersonic range, 11-16 km/s.[1,2]

The majority of the recent work associated with hypersonic flowfields has involved the shock layer; the shock wave precursor, on the other hand, has received little attention. The precursor is the region ahead of the shock wave in which radiation, primarily ultraviolet, emitted by the hot shock layer is reabsorbed by the gas. This absorption of radiation causes a heating of the gas in the precursor and the production of atoms as well as ions through the photoionization and photodissociation reactions. These changes might also in turn affect the gas behind the shock front. For example, the preheating of the gas in the precursor as well as the introduction of electrons and ions could potentially increase the rate at which the gas behind the shock approaches equilibrium. It has also been shown that for certain conditions the absorption of radiation ahead of the shock can cause significant increases in the radia-

Presented as Paper 91-1465 at the AIAA 22nd Fluid Dynamics, Plasma Dynamics, and Lasers Conference, Honolulu, HI, June 24-26, 1991; received July 12, 1991; revision received Oct. 29, 1991; accepted for publication Oct. 29, 1991.

*Associate Engineer, Navigation, Control, and Aeronautics Department, 2400 NASA Road 1. Member AIAA.
†Professor, Aerospace Engineering Department. Associate Fellow AIAA.

tive heating to the body.[3,4] Further, the presence of free electrons in the precursor can significantly affect communications with and identification of entry vehicles.[5,6]

Much of the previous work on shock wave precursors has been performed using shock tubes and shock tunnels.[7-9] A number of computational studies have also been performed.[10-13] The majority of this previous work, however, has involved monatomic gases and is therefore not directly applicable to the Earth's atmosphere.

The studies by Tiwari and Szema[13,14] as well as by Omura and Presley[15,16] involve diatomic gases and therefore are significant to a study of the Earth's atmosphere. Tiwari and Szema calculated the effects of the precursor on the shock layer and the radiative heating of a body entering the hydrogen atmosphere of Jupiter, whereas Omura and Presley conducted a shock tube study of the electron densities ahead of strong shock waves in nitrogen as well as air.

The objective of this study was to develop a technique for predicting the character and magnitude of the chemical and thermal nonequilibrium shock wave precursor ahead of a hypervelocity entry vehicle that includes in detail the mass production due to photodissociation and photoionization of the various species and properly accounts for radiative absorption and emission effects on the internal energy modes of both atomic and diatomic species. A secondary objective was to ascertain the effect of this precursor on the vehicle flowfield.

Radiative Transfer Formulation

In most of the previous work investigating shock wave precursors, several assumptions have been imposed on the radiative transfer calculations. A common assumption has been that the shock layer emits radiation as a black body at the equilibrium temperature behind the shock front.[10,12,17] Also, several of the previous works have utilized a multiple step absorption coefficient model[1,13,14] where, at a given temperature, the species radiative properties have been assumed constant over specific frequency regions. However, since photochemical reactions are being considered, variations in the radiative transfer can cause significant changes in the gas. Likewise, the spectral details are very important in these calculations since the important radiative processes occur over different frequency ranges and the frequency of the photon absorbed as well as the process through which it is absorbed directly affects how the photon energy changes the energy of the gas. Without sufficient spectral detail, it is not possible to ascertain what portion of the radiation absorbed causes photoionization or photodissociation and what portion simply causes an increase in the internal energy of the gas.

Because of the necessity of accurate radiation predictions for the calculation of the photochemical reactions, it was decided that a complete spectrally detailed method of calculating the radiative flux was in order. Thus, an extensively modified version of the program RADICAL was utilized. This program, originally created by Nicolet,[18] allows the user to select the frequency points used for the continuum radiation, so it was possible to obtain the spectral detail necessary for accuracy in the calculation of the photochemical reactions. RADICAL also performs detailed calculations of the atomic line radiation.

RADICAL, like many of the schemes currently used in the calculation of radiative transfer, uses the tangent slab approximation. This assumption is a one-dimensional approximation of the full equation of radiative transfer, which treats the radiation emitted at a point in the gas as if it were emitted by an infinite plane of gas positioned perpendicular to the direction of travel of the radiation. Since the thickness of the shock layer is much smaller than the body dimensions, each point in the shock layer is positioned close enough to the body that the rest of the gas in the radiating shock layer indeed appears to be of infinite extent; therefore, this is a reasonable assumption in the shock layer. The precursor, on the other hand, can extend to distances ahead of the shock that are of the same order of magnitude as the body diameter. Therefore, in the precursor, the radiating shock layer no longer appears to be of infinite extent but instead appears to be a slab of finite diameter.

In the one-dimensional problem, as in the shock layer, absorption is the only method by which the radiation is attenuated as it travels through the gas. Therefore, any decrease in the radiative intensity through the gas can be attributed to absorption, which in turn causes an increase in the energy of the gas equal to the decrease in the radiative energy. Since the shock layer does not appear to be of infinite extent at each point in the precursor, however, the radiation no longer behaves one dimensionally. Consequently, in the precursor the radiative transfer is a three-dimensional problem in which a decrease in the radiative intensity can occur due to the geometry as well as the absorption.

This geometric attenuation in the precursor occurs because the radiative energy emitted by the finite diameter shock layer propagates radially outward into the forward 180 deg semisphere. Therefore, as the energy emitted progresses outward, the area through which it passes increases, thus producing a decrease in the radiative flux. This decrease, however, is not due to absorption by the gas and therefore has no effect on the gas.

Thus, to use RADICAL for the radiation calculations, it was necessary to correct for the geometric attenuation of the radiation. This was done by expressing the radiative flux in the precursor as

$$q_\nu = AF_\nu q_\nu^{TS} \tag{1}$$

where q_ν^{TS} is the radiative flux at the point of interest using the tangent slab approximation and AF_ν is the geometric attenuation factor defined by

$$AF_\nu = \left\{1 - \cos^2(\beta)\,\frac{E_3[(\tau_\nu - \tau_\nu^s)\sec(\beta)] - E_3[\tau_\nu \sec(\beta)]}{E_3(\tau_\nu - \tau_\nu^s) - E_3(\tau_\nu)}\right\} \tag{2}$$

In this expression, β is half of the angle subtended by the body as viewed from the point of interest in the precursor. This expression is derived in detail by Stanley.[19]

In the species continuity and energy equations, the terms involving the radiation appear as a divergence of the flux and are defined to account for the absorption and emission of radiation at a point. However, simple differentiation of Eq. (1) yields

$$\frac{\partial q_\nu}{\partial x} = AF_\nu \frac{\partial q_\nu^{TS}}{\partial x} + q_\nu^{TS} \frac{\partial AF_\nu}{\partial x} \tag{3}$$

In this expression, the first term on the right-hand side is the change in the radiative flux due to the emission and absorption of radiation, and the second term is the change due to the geometry of the problem and should not affect the gas. Therefore, the second term was neglected in the flowfield calculations. Notice that if the second term was included in the species continuity and energy equations, an essentially transparent radiation would appear to be absorbed due to the spatial variation of the attenuation factor.

To properly account for the effects of absorption and emission of radiation on the energy of the gas, it is necessary to have an understanding of how each radiative process physically changes the particles involved. The effects of the absorption and emission of radiative energy on the internal energy modes depend on the type of radiative process as well as the frequency of the photon absorbed or emitted. Radiative processes can be separated into three categories: free-free, bound-bound, and bound-free. While free-free and bound-bound processes cause a change in the energy of the gas with no chemical change, the bound-free processes are associated with chemical reactions in the gas, such as photoionization or photodissociation.

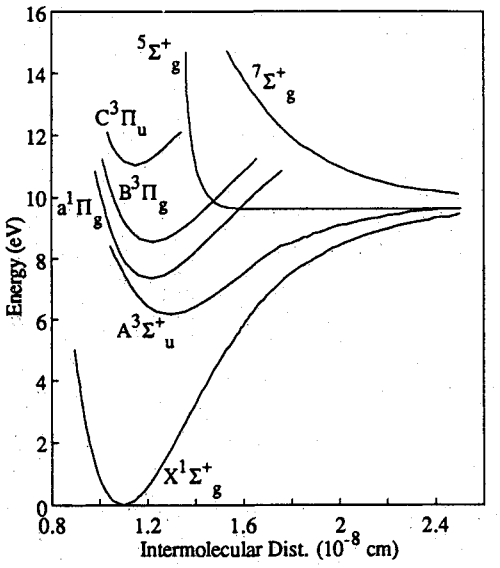

Fig. 1 Potential energy diagram of N_2.

Table 1 Radiative processes included in the shock layer and precursor

	Radiative process	Frequency range
Shock layer		
	Free-free, bremsstrahlung	$0.0<h\nu$
N	Low frequency ionization (highly excited states)	$0.0<h\nu$
	High frequency ionization (ground and first two excited states)	$10.9<h\nu$
	Atomic lines	—
N_2	Birge-Hopfield molecular band	$6.5<h\nu<12.77$
	First positive molecular band	$0.75<h\nu<4.5$
	Second positive molecular band	$0.75<h\nu<4.5$
N_2^+	First negative molecular band	$2.23<h\nu<4.46$
Precursor		
	Free-free, bremsstrahlung	$0.0<h\nu$
N	Low frequency ionization (highly excited states)	$0.0<h\nu$
	High frequency ionization (ground and first two excited states)	$10.8<h\nu$
N_2	Ionization continuum (ground and first three excited states)	$8.24<h\nu$
	Birge-Hopfield molecular band	$6.5<h\nu<12.77$
	First positive molecular band	$0.75<h\nu<4.5$
	Second positive molecular band	$0.75<h\nu<4.5$
	Lyman-Birge-Hopfield molecular band	$4.77<h\nu<9.78$
	Dissociation continuum (adjoining Lyman-Birge-Hopfield molecular band)	$9.78<h\nu$
N_2^+	First negative molecular band	$2.23<h\nu<4.46$

Photodissociation of the relatively cool nitrogen in the precursor occurs through a process called predissociation, a radiationless process in which a molecule makes a transition from a discreet electronic state to a dissociated state.[20] In cool nitrogen, this predissociation occurs primarily through the Lyman-Birge-Hopfield molecular band and the subsequent transfer out of the $a^1\Pi_g$ state into the repulsive $^5\Sigma^+_g$ + state (Fig. 1).

The radiative processes included in the calculation of the emission and absorption in the shock layer and precursor for this study are given in Table 1. The radiative processes included in the shock layer are those originally accounted for in the modified version of RADICAL. These processes include not only the continuum processes but also the atomic lines associated with the nitrogen atom. Since only continuum processes were included in the precursor, the continuum mechanisms originally included in RADICAL were retained. Also, the photoionization of molecular nitrogen, the Lyman-Birge-Hopfield molecular band, and the dissociation of molecular nitrogen through a continuum adjoining the Lyman-Birge-Hopfield band were added to the processes in RADICAL.

The absorption coefficients for photoionization of molecular nitrogen and the Lyman-Birge-Hopfield molecular band were determined using theoretical expressions derived according to Zel'dovich and Raizer.[21] For the photoionization process, the absorption coefficient was found to be given by the expression

$$k_\nu = 1.9986 \times 10^{-14} \frac{N_{N2}}{(h\nu)^3} \sum_{j=j^*}^{\infty} \frac{1}{j^3} e^{-(x_1 - x_j)} \tag{4a}$$

$$x_j = \frac{(I_{N2} - E_{elct_j})}{kT} \tag{4b}$$

where the photon energy $h\nu$ is given in electron volts. The lower limit on the summation over the electronic states in this equation is governed by the requirement that the photon energy be greater than the binding energy for the state. Otherwise, the photon has insufficient energy to cause photoionization.

For this study, the summation in Eqs. (4) was limited to the lowest four electronic states of the nitrogen molecule. However, in the cool precursor the populations of all except the ground electronic state were small. It should be noted that Eqs. (4) provide values near the ionization threshold on the same order of magnitude as those predicted by Zel'dovich and Raizer[22] as well as those predicted by Marr.[23]

The absorption coefficient for the Lyman-Birge-Hopfield molecular band was found to be given by

$$k_\nu = 9.1458 \times 10^{16} \frac{N_{N2}}{T} \exp\left[-\frac{(113{,}314.97 - 11{,}610.14 h\nu)}{T}\right] \tag{5}$$

This equation was obtained from expressions given by Zel'dovich and Raizer[21] using an absorption oscillator strength of 3.7×10^{-6} from Allen[24] and then correcting to match experimental predictions given by Watanabe.[25] The absorption coefficient for the dissociation continuum adjoining this molecular band was assumed to be given by the expression

$$k_\nu = 4.97 \times 10^{-20} N_{N2} \tag{6}$$

The constant in this equation was taken from the data presented by Watanabe for absorption through this process in cool air.

Precursor Formulation

For this study, the Earth's atmosphere was modeled as pure nitrogen rather than a nitrogen oxygen mixture. This approach is a common simplifying assumption when performing nonequilibrium, hypervelocity flowfield calculations since a nitrogen gas represents the properties of air quite well. In dealing with the precursor, however, the primary concern was whether or not the absorption processes of nitrogen sufficiently model those of air. After careful consideration it was decided that due to the predominance of nitrogen in the atmosphere it would be reasonable to represent the atmosphere as nitrogen in this initial study.

The effects of thermal nonequilibrium in the precursor were included in this study by permitting the free electrons and heavy particles to have different temperatures. Further, it was assumed that the free electrons and electronic states were in equilibrium at a common temperature, which, as discussed by Nelson and Goulard,[11] is one of the limiting cases for the precursor. For this region of the gas, the temperature governing the electronic states would normally be expected to be greater than the heavy particle temperature but less than the electron temperature. Thus, ideally a three temperature model should be used allowing a separate electronic temperature.

Nevertheless, since the mechanisms and expressions for the transfer of energy between the electronic states and the free electrons are not well known or well understood, it was decided to use only a two temperature model. However, to correct for the local thermodynamic nonequilibrium between the electrons and the electronic states, a collision limiting correction[26] was applied to the populations of the molecular electronic states when computing the radiative emission and absorption phenomena.

For this study, the mass production rates in the precursor due to collisional reactions were neglected in comparison with those due to photochemical reactions. The photoreactions used in the precursor include the dissociation of molecular nitrogen and the ionization of both molecular and atomic nitrogen, i.e.,

$$N_2 + h\nu \leftrightarrow^{k_{\nu 1}} 2N$$

$$N_2 + h\nu \leftrightarrow^{k_{\nu 2}} N_2^+ + e^-$$

$$N + h\nu \leftrightarrow^{k_{\nu 3}} N^+ + e^-$$

The elastic collisional terms in the electron/electronic energy equation were evaluated using the collisional cross sections of Gnoffo et al.[27]

The effects of the absorption of radiation through free-free and bound-bound processes were also included in this study. Although these processes do not cause chemical reactions, they do cause an increase in the energy of the gas, and their effects must be included in the electron/electronic energy equation. Absorption through atomic lines was neglected due to the expected low concentration of atomic species.

The equations governing the fluid properties on the stagnation streamline in the precursor are the steady, one-dimensional, nonequilibrium Euler equations.

Global continuity:

$$\frac{\partial}{\partial x}(\rho V) = 0 \tag{7}$$

Momentum:

$$\rho V \frac{\partial V}{\partial x} + \frac{\partial p}{\partial x} = 0 \tag{8}$$

Energy:

$$\rho V \frac{\partial H}{\partial x} + \frac{\partial q}{\partial x} = 0 \tag{9}$$

In Eq. (9), H is the total enthalpy of the gas defined in terms of the static enthalpy such that

$$H = h + \tfrac{1}{2}V^2 \tag{10}$$

where

$$h = \frac{p}{\rho} + \sum_{n=1}^{n_s}(e_{\mathrm{tr}_n} + e_{\mathrm{rot}_n} + e_{\mathrm{vib}_n} + e_{\mathrm{elct}_n} + e_n^0) \tag{11}$$

The second term in Eq. (9) is the gradient of the radiative flux. This term accounts for the increase or decrease in the energy of the gas due to absorption and emission of radiation. In addition to these equations, the equation of state for a two temperature gas is required,

$$p = \rho \hat{R} T \sum_{n=1}^{n_s}\left(\frac{\rho_n}{\rho}\frac{1}{M_n}\right) + \rho \frac{\hat{R}}{M_{e^-}}\frac{\rho_{e^-}}{\rho}(T_e - T) \tag{12}$$

To allow for the effects of thermal nonequilibrium, an electron/electronic energy equation was added to these equations,

$$\frac{\partial}{\partial x}(\rho V e_e'') = -p_e \frac{\partial V}{\partial x} + \sum_{n=1}^{n_s}\xi_{e,n} + \dot{w}_e \frac{V^2}{2} - \frac{\partial q}{\partial x} + \sum_{i=1}^{n_{\mathrm{diss}}}\int_0^\infty \frac{Y_{\nu_i}^p(h\nu - \Delta E_{\mathrm{elct}_i} - D_i)}{h\nu}\frac{\partial q_\nu}{\partial x}\,d\nu + \sum_{i=1}^{n_{mb}}\int_0^\infty \frac{Y_{\nu_i}^p(h\nu - E_{\mathrm{elct}_i}^{\mathrm{upp}} + E_{\mathrm{elct}_i}^{\mathrm{low}})}{h\nu}\frac{\partial q_\nu}{\partial x}\,d\nu \tag{13}$$

where

$$e_e'' = \frac{\rho_{e^-}}{\rho}e_{e^-} + \sum_{n=1}^{n_s}(e_{\mathrm{elct}_n} + e_n^0) \tag{14}$$

In this equation, e_{e^-} is the kinetic energy of the free electrons, $3/2kT_e/m_{e^-}$, whereas e_{elct_n} and e_n^0 are the electronic and zero point energies of the nth species. The last three terms on the right-hand side of Eq. (13) allow for the effects of the absorption of radiation. This equation is derived in detail in Ref. 19.

Chemical nonequilibrium was accounted for in the precursor through the addition of a species continuity equation for each of the five species in the problem. These equations are of the form

$$\rho V \frac{\partial(\rho_n/\rho)}{\partial x} = -m_n \int_0^\infty \frac{Y_{\nu_n}^s}{h\nu}\frac{\partial q_\nu}{\partial x}\,d\nu \tag{15}$$

where

$$Y_{\nu_{N_2}}^s = -\frac{k'_{\nu_1} + k'_{\nu_2}}{k'_{\nu_{\mathrm{tot}}}} \tag{16a}$$

$$Y_{\nu_{N_2^+}}^s = \frac{k'_{\nu_2}}{k'_{\nu_{\mathrm{tot}}}} \tag{16b}$$

$$Y_{\nu_N}^s = \frac{2k'_{\nu_1} - k'_{\nu_3}}{k'_{\nu_{\mathrm{tot}}}} \tag{16c}$$

$$Y_{\nu_{N^+}}^s = \frac{k'_{\nu_3}}{k'_{\nu_{\mathrm{tot}}}} \tag{16d}$$

$$Y_{\nu_{e^-}}^s = \frac{k'_{\nu_2} + k'_{\nu_3}}{k'_{\nu_{\mathrm{tot}}}} \tag{16e}$$

The term on the right-hand side of Eq. (15) is the mass production rate of the nth species due to photoprocesses. The absorption coefficients, k'_{ν_1}, k'_{ν_2}, and k'_{ν_3} are those for the absorption and emission processes associated with each of the three photochemical reactions discussed previously. Equation (15) is derived in detail in Ref. 19.

In all of the previous equations, the radiative terms $\partial q/\partial x$ are the changes in the radiative flux due only to the absorption of radiation and not those due to the geometry of the problem as discussed in the previous section.

The equations governing the flowfield properties in the precursor were solved using a space marching technique starting at a point far from the shock front and marching in toward the shock wave. The point furthest from the shock wave was assumed to be far enough from the radiating shock layer that the ultraviolet radiation was absorbed between this point and the shock; thus the gas properties at this point were forced to remain at the freestream conditions. The spacing between each spatial point was adjusted as the solution progressed to prevent the changes in the flowfield properties between each point from becoming too large. This procedure forced a large concentration of points in the regions of large gradients and allowed the distance between the points to increase in regions of small gradients. At each individual point in the precursor, the governing equations, Eqs. (7–16), were solved using an iterative procedure.

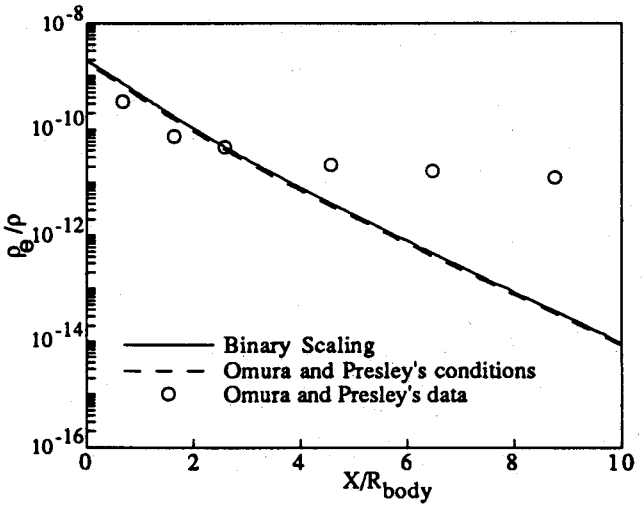

Fig. 2 Comparison between current method and shock tube data from Omura and Presley.[15,16]

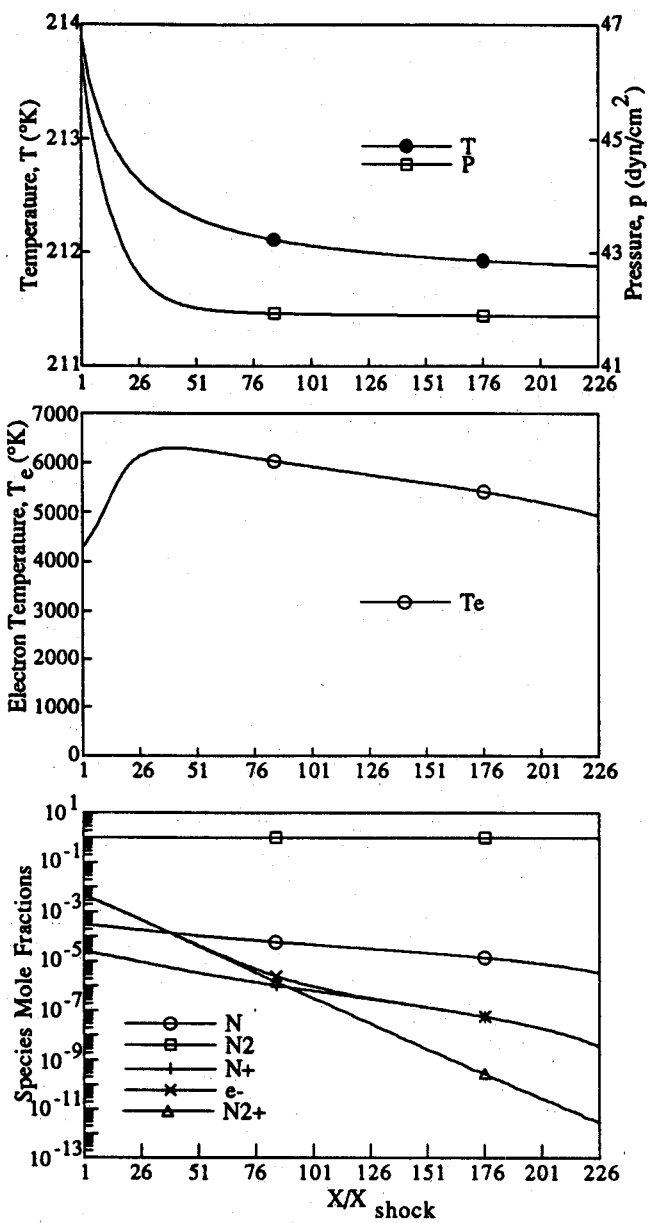

Fig. 3 Precursor profiles for 16 km/s case at 72 km altitude.

Shock Layer Formulation

To properly model the precursor ahead of a shock wave, it is necessary to know the spectral details of the radiation that passes from the shock layer and through the shock front to the precursor. To calculate these spectral details, the conditions of the gas in the shock layer must be known in detail. For the flight conditions of interest in this study, a number of important phenomena such as chemical and thermal nonequilibrium must be included to properly model the shock layer. Also, since the effects of radiation are of primary importance in the precursor, it is desirable that they be included in the shock layer model. The inclusion of these three phenomena can significantly affect the radiation and hence the precursor.

For this portion of the flowfield, a viscous shock layer (VSL) scheme based on a version of the NASA code VSL3DNQ[28] was used. The version of VSL3DNQ used in this study was modified extensively by Carlson.[29] These modifications primarily involved the nonequilibrium chemistry and the effects of thermal nonequilibrium. However, the code was also modified to allow the shock layer and radiation calculations to be coupled to the gas dynamics, thus incorporating the effects of the emission and absorption of radiation into the flowfield solution.

Results and Discussion

Figure 2 compares the electron mass fractions found by Omura and Presley[15,16] in the precursor ahead of a shock wave in a nitrogen gas with those calculated using the present method. Omura and Presley measured the electron densities in the precursor using a 12-in. shock tube. The shock velocity for their case was 11.89 km/s. Shown in this figure, along with Omura and Presley's results, are two curves showing the electron mass fractions calculated using the current method. The dashed curve was calculated using Omura and Presley's freestream conditions and shock velocity with a 12-in.-diam body. However, the solid curve was calculated using a lower freestream density and pressure than Omura and Presley along with a larger diameter body scaled so that the conditions match those of Omura and Presley's case using binary scaling.

As can be seen from this figure, the electron mass fractions calculated using this method match those found by Omura and Presley reasonably well near the shock front. However, far from the shock they deviate. It is believed that the differences in the electron mass fraction far from the shock are due to the reflection of the radiative flux off of the shock tube walls in the Omura and Presley case. This reflection should greatly increase the quantity of radiation present far ahead of the shock wave over that which would be present in a free field such as is being used for the calculations. This increased presence of radiation far from the shock would induce greater absorption and thus an increase in the production of electrons due to photoionization. It is also interesting to note how well the two sets of calculations match using binary scaling.

The results discussed in the remainder of this section are representative of "typical" conditions for an aerobrake vehicle entering the Earth's atmosphere upon return from Mars. These results were calculated for the stagnation streamline of a 2.3 m nose radius vehicle at three altitudes: 72, 75, and 80 km. The shock layer calculations were made using 52 points between the shock wave and the body and allowing for atomic local thermodynamic nonequilibrium as well as radiation/gas-dynamic coupling. The radiation calculations were made using 74 continuum frequency points selected to provide good spectral detail in the ultraviolet absorption region of interest in the precursor. A wall temperature of 1650 K was used in both the shock layer and the radiation calculations.

72 km, 16 km/s

Figure 3 shows the heavy particle temperature, electron/electronic temperature, pressure, and the five species mole fraction variations through the precursor for this case. The

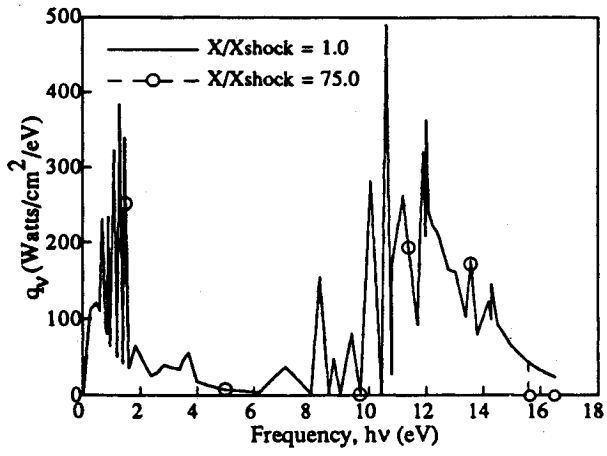

Fig. 4 Radiative transfer for 16 km/s case at 72 km altitude.

radiative flux through the shock front for this case was 1385.0 W/cm^2, and the spectral details of this radiation are shown in Fig. 4. The shock standoff distance for this case was 6.60 cm. The radiation emitted from the shock layer for this case was the greatest of all of those considered. Thus this case experienced the largest flowfield perturbations in the precursor region.

From these figures, it can be seen that the heavy particle temperature and pressure increased steadily through the precursor region. However, even for this extreme case the changes in these values were small. The density and velocity of the gas were found to be essentially constant in the precursor. This behavior verifies what was shown by Tiwari and Szema[13,14] and assumed by many others.[10-12,15]

The electron/electronic energy of the gas also increased from a value of essentially zero in the freestream to a value on the order of 10^9 immediately ahead of the shock front. It was observed from comparisons of the total energy increase in the precursor to the electron/electronic energy increase that 99% of the radiative energy absorbed affected the electron/electronic energy of the gas. Only 1% of the energy absorbed affected the heavy particle translational, rotational, and vibrational energies of the gas. Furthermore, by comparing the increase in the zero point energy of the gas with the increase in the electron/electronic energy, it was found that 96% of the increase in the electron/electronic energy was involved with an increase in the zero point energy. From this, it was found that the majority of the energy absorbed in the precursor was involved with the ionization and dissociation of the gas.

The electron/electronic temperature behaved differently in the precursor than the other gas properties. It increased steadily to a maximum value of approximately 6300 K at a distance of 40 shock standoff distances ahead of the body. It then decreased rapidly to a value of 4290 K immediately ahead of the shock front. This decrease in the electron/electronic temperature was a result of the production of "low" energy electrons through photoionization caused by photons of frequencies only slightly larger than the ionization threshold of N_2. The production of these low energy electrons caused a decrease in the average energy per electron, hence a decrease in the electron/electronic temperature. That this decrease was a result of the production of low energy electrons rather than due to a transfer of energy from the electrons through elastic collisions was evident since there was no decrease in the electron/electronic energy accompanying this decrease in the electron/electronic temperature. This decrease also coincided with a region of rapid increase in the electron concentration in the gas due to the photoionization of molecular nitrogen.

The photons with energy near the ionization threshold of molecular nitrogen were absorbed rapidly in front of the shock since the strongest absorption region for an ionization process is at frequencies near the threshold. The higher energy photons in the weaker absorption range, far from the threshold, escaped to distances further from the shock where they were absorbed, causing the creation of high energy electrons. The production of these high energy electrons resulted in a high electron/electronic temperature far from the shock. However, although the electron/electronic temperature was high far from the shock, the electron mass fraction in this region was extremely small. It should be noted that a similar decrease in the precursor electron temperature near the shock was also predicted by Foley and Clarke,[12] although they attributed it to collisional electron impact ionization.

Considering the mole fractions of the five species, it can be seen that the dominant chemical reaction far from the shock was the photoionization of atomic nitrogen. However, near the shock, photoionization of molecular nitrogen dominated. The mole fractions of the ionized nitrogen molecule immediately ahead of the shock were at least an order of magnitude greater than those for the nitrogen atom and ionized nitrogen atom, although there were significant quantities of all three species.

Because the dominant change in the precursor was due to the photoionization of molecular nitrogen, the thickness of the precursor was considered to be the distance through which this reaction had an effect. By this definition, for this case the shock precursor thickness was in the range of 75 shock standoff distances or 495 cm. Although there was a slight heating of the gas as well as the production of nitrogen atoms through photodissociation at greater distances from the shock, their effects were small compared with the changes within 495 cm of the shock front.

As can be seen in Fig. 4, the radiation propagating through the shock wave from the shock layer into the precursor was distributed over a wide range of frequencies. A large portion of this radiative energy was in the infrared frequency range ($h\nu \leq 5$ eV). Most of the radiation in this region was emitted by the entry body itself, although embedded within the continuum radiation from the body were a number of atomic lines. Also, the peak of radiation near 3.5 eV was due to three molecular bands, the first negative band of N_2^+ and the first and second positive bands of N_2. There was also a large quantity of radiative energy in the ultraviolet frequency range. That above 10 eV was due primarily to the Birge-Hopfield band of molecular nitrogen as well as the ionization continuum and lines of atomic nitrogen. Through the visible frequency ranges (5 eV $\leq h\nu \leq$ 8 eV) there was very little radiative energy.

The second curve in Fig. 4 shows the radiative flux at a position 75 shock standoff distances ahead of the shock front uncorrected for the geometric attenuation. By comparing this uncorrected radiative flux with the radiative flux through the shock front, it is possible to ascertain in what portion of the frequency range the cool precursor absorbed. This figure shows that the precursor absorbed radiation strongly at frequencies above the ionization threshold of molecular nitrogen, 15.59 eV. Although there was energy absorbed at frequencies less than this threshold due to photodissociation of molecular nitrogen and photoionization of atomic nitrogen, the amount of energy absorbed in these processes was small compared with that absorbed in the photoionization of molecular nitrogen. This result agrees with the previous statements that the dominant reaction was molecular ionization.

Through the course of this study it was found that even though there was significant production of dissociated and ionized nitrogen in the precursor region, the precursor had very little effect on the gas in the shock layer. By including these perturbed preshock conditions in the viscous shock layer calculations, it was found that they had negligible effect on the shock layer solution and produced no measurable change in the radiative heat transfer to the body. The primary change due to the inclusion of the precursor was in the conditions of the gas immediately behind the shock wave. Neglecting the

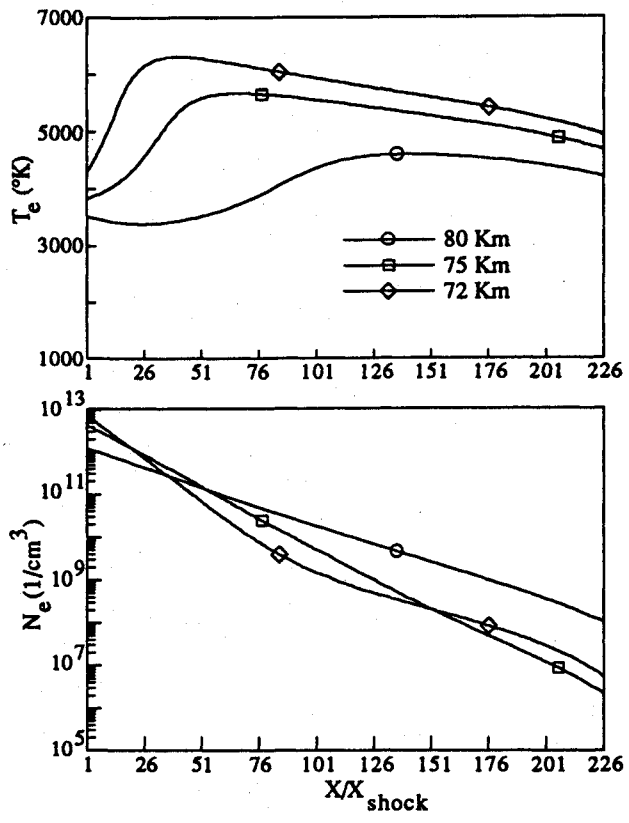

Fig. 5 Variation of the precursor flowfield with changes in altitude.

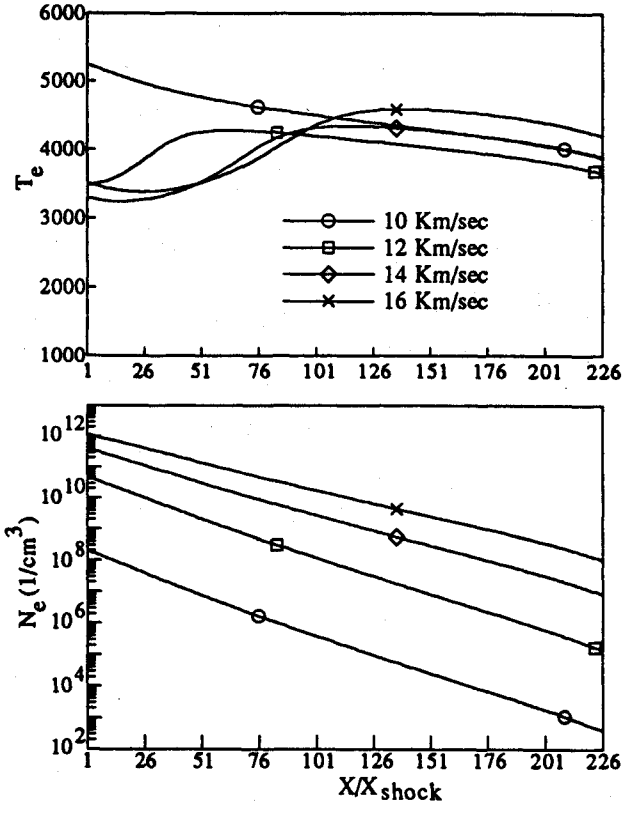

Fig. 6 Variation of the precursor flowfield with changes in freestream velocity.

Table 2 Shock standoff distances and radiative fluxes

V, km/s	Alt., km	X_{shock}, cm	q_{shock}, W/cm^2
16	72	6.60	1385.0
16	75	6.72	776.2
16	80	7.25	264.5
14	80	8.69	126.9
12	80	10.17	65.9
10	80	11.14	54.2

precursor, the mass fractions for the free electrons, ions, and atoms were zero upon crossing the shock; however, including the effects of the precursor, these mass fractions had nonzero values. Likewise, including the effects of the precursor resulted in a slight increase in the electron temperature in the region immediately behind the shock front. However, within two spatial points of the shock front the shock layer solutions with and without the precursor agreed.

Parametric Studies

Figure 5 shows the electron number densities and the electron/electronic temperature in the precursor for three cases. All three of these cases were at a velocity of 16 km/s; however, each case was at a different altitude: 72, 75, and 80 km. The shock standoff distance and radiative flux through the shock front for each of these cases are presented in Table 2.

From these figures, it can be seen that for a constant velocity the magnitude of the changes in the precursor increased with decreasing altitude. This inverse relationship corresponds with trends observed by Dobbins[17] and was a result of two factors. First and foremost, as shown in Table 2, with the decrease in altitude the radiative flux through the shock increased due to an increase in the extent of the equilibrium region in the shock layer. Second, with the increase in density at the lower altitudes, a larger percentage of the radiation passing through the shock was absorbed before being attenuated due to the geometry.

It should also be noted that as the altitude decreased, the length of the precursor region decreased. This change was a result of the increased density at the lower altitudes, which caused the radiative mean free paths to decrease. Hence, the radiation was absorbed in a shorter distance ahead of the shock. This trend was also predicted by previous studies.[11]

Figure 6 shows the electron number densities and electron/electronic temperature for four cases. All of these cases were at an altitude of 80 km, and the freestream velocities ranged from 10 to 16 km/s. The shock standoff distance and radiative flux through the shock front for each of these cases are presented in Table 2.

From these figures, it can be seen that, at a constant altitude, as the freestream velocity increased the magnitude of the electron number densities in the precursor also increased. This trend was a result of the increase in the equilibrium temperature in the shock layer as the velocity increased and the accompanying rise in the radiative flux through the shock front; this trend is also in agreement with the results and predictions of previous researchers.[16,17] The precursor thickness also increased with velocity, again as a result of the increased radiative flux with velocity. As the radiative energy passing through the shock increased, a larger distance was required for this energy to be absorbed or attenuated ahead of the shock.

The increase in the velocity had varied effects on the electron/electronic temperature, however. The electron/electronic temperature at the shock decreased with velocity from 10 to 14 km/s. However, from 14 to 16 km/s it increased. This varied effect is due to differences in the quantity of low energy electrons created immediately ahead of the shock due to the ionization of molecular nitrogen. In fact, at 10 km/s there was insufficient ionization of molecular nitrogen ahead of the shock to cause a decrease in the electron/electronic temperature.

Conclusions

In this paper, a model for predicting the magnitude and characteristics of the shock wave precursor ahead of a hypervelocity vehicle in the Earth's atmosphere has been presented. This model treats the Earth's atmosphere as a nitrogen gas. This method includes detailed mass production for photodissociation and photoionization and accounts for the effects of emission and absorption on the individual energy modes of the gas. This technique includes the effects of both chemical and thermal nonequilibrium in the flowfield as well as, in the radiative flux calculations, the consequences of local thermodynamic nonequilibrium for the molecular species.

This method has been used to determine the shock wave precursor ahead of vehicles entering the Earth's atmosphere upon return from Mars. Comparison of the results with previous shock tube studies has shown that the method provides reasonably accurate results. The test cases have shown that there is significant production of atoms, ions, and electrons ahead of the shock front and that the precursor is characterized by molecular ionization and an enhanced electron/electronic temperature. However, for the conditions considered in this study, the precursor has negligible effect on the subsequent shock layer flowfield. For flowfield calculations around entry vehicles at greater velocities or which penetrate deeper into the Earth's atmosphere at similar velocities to those studied here, the precursor could be significant. However, even at the conditions considered in this study, the free electrons present in the precursor could have significant impact on communication with the entry vehicle.

Acknowledgment

This work was primarily supported by NASA Grant-1-1003 from the NASA Langley Research Center, with Lin C. Hartung acting as technical monitor.

References

[1]Smith, G. L., "Radiation-Induced Precursor Flow Field Ahead of a Reentering Body," Ph.D. Dissertation, Virginia Polytechnic Inst. and State Univ., Blacksburg, VA, March 1968.

[2]Williams, S. D., Pavlosky, J. E., and Curry, D. M., "A Preliminary TPS Design for MRSR-Aerobraking at Mars and at Earth," AIAA Paper 90-0052, Jan. 1990.

[3]Lasher, L. E., and Wilson, K. H., "Effects of Shock Precursor Heating on Radiative Flux to Blunt Bodies," NASA-CR-1265, 1969.

[4]Tiwari, S. N., and Szema, K. Y., "Effects of Precursor Heating on Chemical and Radiative Nonequilibrium Viscous Flow Around a Jovian Entry Body," AIAA Paper 78-907, May 1978.

[5]Wetzel, L., "Far-Flow Approximation for Precursor Ionization Profiles," *AIAA Journal,* Vol. 2, No. 7, 1964, pp. 1208–1214.

[6]Lederman, S., and Wilson, D. S., "Microwave Resonant Cavity Measurements of Shock Produced Electron Precursor," *AIAA Journal,* Vol. 5, No. 1, 1967, pp. 71–77.

[7]Shreffler, R. G., and Christian, R. H., "Boundary Disturbances in High Explosive Shock Tube," *Journal of Applied Physics,* Vol. 25, No. 3, 1954, pp. 324–331.

[8]Voorhies, H. G., and Scott, F. R., "Optical Measurements in a Helium Shock Tube," *Bulletin of the American Physical Society,* Vol. 4, 1959, p. 40.

[9]Weymann, H. D., "Electron Diffusion Ahead of Shock Waves in Argon," *Physics of Fluids,* Vol. 3, No. 4, 1960, pp. 545–548.

[10]Murty, S. S. R., "Effects of Line Radiation on Precursor Ionization," *Journal of Quantitative Spectroscopy and Radiative Transfer,* Vol. 8, Sept. 1968, pp. 531–554.

[11]Nelson, H. F., and Goulard, R., "Structure of Shock Waves with Nonequilibrium Radiation and Ionization," *Physics of Fluids,* Vol. 12, No. 8, 1969, pp. 1605–1617.

[12]Foley, W. H., and Clarke, J. H., "Shock Waves Structured by Nonequilibrium Ionizing and Thermal Phenomena," *Physics of Fluids,* Vol. 16, No. 3, 1973, pp. 373–383.

[13]Tiwari, S. N., and Szema, K. Y., "Radiation Induced Precursor Flow Field Ahead of a Jovian Entry Body," AIAA Paper 77-768, June 1977.

[14]Tiwari, S. N., and Szema, K. Y., "Influence on Precursor Heating of Viscous Flow Around a Jovian Entry Body," AIAA Paper 78-190, Jan. 1978.

[15]Omura, M., and Presley, L. L., "Electron Density Measurements Ahead of Shock Waves in Air," *AIAA Journal,* Vol. 7, No. 12, 1969, pp. 2363–2365.

[16]Omura, M., and Presley, L. L., "Further Studies of Precursor Electron Densities Ahead of Shock Waves," *Proceedings of the 4th Plasma Sheath Symposium,* NASA-SP-252, Oct. 1970, pp. 335–358.

[17]Dobbins, R. A., "Photoexcitation and Photoionization of Argon Ahead of a Strong Shock Wave," AIAA Paper 68-666, June 1968.

[18]Nicolet, W. E., "Advanced Methods for Calculating Radiation Transport in Ablation Product Contaminated Boundary Layers," NASA-CR-1656, Sept. 1970.

[19]Stanley, S. A., "The Effects of Shock Wave Precursors Ahead of Hypersonic Entry Vehicles," M.S. Thesis, Texas A&M Univ., College Station, TX, Dec. 1990.

[20]Herzberg, G., *Molecular Spectra and Molecular Structure, I. Spectra of Diatomic Molecules,* 2nd ed., Krieger, Malabar, FL, 1989.

[21]Zel'dovich, Y. B., and Raizer, Y. P., *Physics of Shock Waves and High-Temperature Phenomena,* Vol. 1, Academic, New York, 1966.

[22]Zel'dovich, Y. B., and Raizer, Y. P., *Physics of Shock Waves and High-Temperature Hydrodynamic Phenomena,* Vol. 2, Academic, New York, 1967.

[23]Marr, G. V., *Photoionization Processes in Gases,* Academic, New York, 1967.

[24]Allen, R. A., "Air Radiation Graphs: Spectrally Integrated Fluxes Including Line Contributions and Self Absorption," NASA-CR-556, 1965.

[25]Watanabe, K., "Ultraviolet Absorption Processes in the Upper Atmosphere," *Advances in Geophysics,* Vol. 5, 1958, pp. 153–221.

[26]Horton, T. E., "Radiative Coupled Nonequilibrium Flow Fields Associated with Aeroassisted Orbital Transfer," Univ., of Mississippi, NASA CR NAG-1-496, University, MS, March 1986.

[27]Gnoffo, P. A., Gupta, R. N., and Shinn, J. L., "Conservation Equations and Physical Models for Hypersonic Air Flows in Thermal and Chemical Nonequilibrium," NASA-TP-2867, Feb. 1989.

[28]Thompson, R. A., "Comparison of Nonequilibrium Viscous Shock Layer Solutions with Windward Surface Shuttle Heating Data," AIAA Paper 87-1473, June 1987.

[29]Carlson, L. A., "Nonequilibrium Radiation and Chemistry Models for Aerocapture Vehicle Flowfields," Texas A&M Univ., TAMRF Rept. No. 6382-90-02, College Station, TX, June 1990.

Ernest V. Zoby
Associate Editor